

## Parameter clustering in Bayesian functional PCA of fMRI data

Nicolò Margaritella\*, Vanda Inácio De Carvalho, and Ruth King

University of Edinburgh, School of Mathematics,  
James Clerk Maxwell Building, The King's Buildings,  
Peter Guthrie Tait Road, Edinburgh, UK

\**email*: N.Margaritella@sms.ed.ac.uk

**SUMMARY:** The extraordinary advancements in neuroscientific technology for brain recordings over the last decades have led to increasingly complex spatio-temporal datasets. To reduce oversimplifications, new models have been developed to be able to identify meaningful patterns and new insights within a highly demanding data environment. To this extent, we propose a new model called Parameter clustering functional Principal Component Analysis (PCl-fPCA) that merges ideas from Functional Data Analysis and Bayesian nonparametrics to obtain a flexible and computationally feasible signal reconstruction and exploration of spatio-temporal neuroscientific data. In particular, we use a Dirichlet process Gaussian mixture model to cluster functional Principal Component scores within the standard Bayesian functional PCA framework. This approach captures the structure of spatial dependence among smoothed time series (curves) and its interaction with the time domain without imposing a prior spatial structure to the data. Moreover, by moving the mixture from data to functional principal component scores, we obtain a more general clustering procedure, thus allowing a higher level of intricate insight and understanding of the data. We present results from a Monte Carlo simulation study showing improvements in curve and correlation reconstruction compared with different Bayesian and frequentist fPCA models and we apply our method to a resting-state fMRI data analysis providing a rich exploration of the spatio-temporal dependence in brain time series.

**KEY WORDS:** Bayesian hierarchical model; Clustering; Dirichlet process; Functional data analysis; Neuroscientific data; Spatio-temporal data.

## 1. Introduction

Several tools for the recording of different brain processes, such as functional Magnetic Resonance Imaging (fMRI) and Electroencephalogram (EEG) produce remarkable amounts of spatio-temporal data which challenge researchers to find suitable models for increasingly complex datasets. Consequently, the last decade has seen a marked increase in flexible methods for high dimensional data in neuroscience. Functional Data Analysis (FDA) is a fairly recent research field in statistics concerned with the analysis of data providing information about curves, shapes and images which vary over a continuum, usually time or space (see Ramsay and Silverman (2005) for an overview). In the FDA framework, data can be considered as noise-corrupted, discretised realisations of underlying smooth functions (curves or trajectories) which are recovered using basis expansions and smoothing (Ramsay et al., 2009). Many standard statistical tools have been translated into the FDA framework. Functional PCA (fPCA) is a technique that defines a set of smooth trajectories as an expansion of orthonormal bases (eigenfunctions) and weights which are called functional Principal Component scores (fPC scores, Ramsay and Silverman, 2005, Section 7). One of the advantages of fPCA is that it can be conveniently represented as a hierarchical mixed model in the Bayesian setting, with the joint posterior distribution of the fPC scores being the main target of inference (Crainiceanu and Goldsmith, 2010).

There has been a growing interest in applying FDA to neuroscientific data (see, among others, Hasenstab et al., 2017; Tian, 2010; Viviani et al., 2005). Often, in the FDA literature, underlying random curves are assumed to be independent and their correlation is ignored if believed to be mild (Liu et al., 2017). However, curve dependence is of particular importance in the analysis of brain activity because of the complex architecture of spatio-temporal connections between brain areas (Wolfson, 2018). Recently, Liu et al. (2017) considered spatial dependence among trajectories by modelling the covariance of the fPC scores within a

frequentist approach. Their results showed significant improvements in curves reconstruction compared to the standard approach assuming independence, especially with low signal-to-noise ratios.

The present study introduces a new method for the analysis of functional data in neuroscience. We develop a modified version of the Bayesian fPCA model (Crainiceanu and Goldsmith, 2010) called Parameter Clustering fPCA (PCI-fPCA) that makes use of a Dirichlet Process (DP) mixture (Rasmussen, 2000; Neal, 2000; Escobar and West, 1995) to model the prior distribution of the fPC scores. Different functional mixture models that cluster functions through clustering of the coefficients in a basis expansion have been proposed in the literature (Angelini et al., 2012; Ray and Mallick, 2006; Zhou and Wakefield, 2006; James and Sugar, 2003). In our work we use the principal component bases due to their straightforward interpretation and employ independent DP mixture priors for every eigendimension retained. By allowing different clustering of the fPC scores for each eigendimension retained, we avoid the limitations of assuming separability of the cross-covariance and any a priori spatial covariance structure of the data, obtaining further insights from space-time interactions. We show that our approach has multiple advantages in the analysis of neuroscientific data as it improves curve reconstruction thanks to the local borrowing of information compared to current fPCA approaches; it offers further insights into the spatio-temporal structure of the data as a result of dimension-specific curve classification; and it can be defined as a simple and computationally feasible hierarchical model which can be easily implemented in **R**.

The rest of the paper is structured as follows: in Section 2 we overview the standard Bayesian fPCA model and introduce the new method, along with computational details. Section 3 reports the setting and results of a Monte Carlo simulation study where we compare the performance of PCI-fPCA with standard Bayesian and frequentist fPCA approaches under different data generating processes and noise levels. In all scenarios our model showed

improvements in both curve reconstruction and their correlation, especially in the case of low signal-to-noise ratio. Section 4 addresses the application of our method to a resting-state fMRI dataset recorded from a healthy subject and we discuss the further insights obtained in the spatio-temporal structure of the data and the underlying neurophysiological processes. Conclusions are discussed in Section 5.

## 2. Methods

### 2.1 Bayesian Functional PCA

The standard FDA model is given by

$$Y_{it} = X_{it} + \epsilon_{it}, \quad (1)$$

where  $Y_{it}$  denote the noise-corrupted, discretised observed data for every spatially-correlated region (trajectory)  $i = 1, \dots, n$  and time point  $t = 1, \dots, T$ ;  $X_{it}$  the associated underlying random curve and  $\epsilon_{it}$  the noise term with zero mean and precision  $\tau$ .

Functional PCA assumes that the process  $X_t$  can be represented by the Karhunen-Loève expansion so that each realisation  $X_{it}$  takes the form

$$X_{it} = \mu_t + \sum_{k=1}^{\infty} \xi_{ik} \phi_{kt}, \quad i = 1, \dots, n \quad t = 1, \dots, T, \quad (2)$$

where  $\mu_t$  represents a population average and the infinite sum is a linear combination of orthonormal eigenfunctions  $\phi_{kt}$ , which are usually assumed to be observed, and fPC scores  $\xi_{ik}$ , which are the main goal of inference. Even if the number of eigendimensions can also be modelled with an appropriate distribution (see, for example, Suarez et al., 2017), in practice only  $K$  pre-determined terms of the linear expansion are retained pertaining to those that explain a sufficiently large part of the total variability in the data (Sørensen et al., 2013). Often the case  $\mu_t = 0$  is assumed and the centered data  $\tilde{Y}_{it}$  are obtained by subtracting an estimate  $\hat{\mu}_t$  of the population average (Crainiceanu and Goldsmith, 2010).

The fPC scores  $\xi_{ik}$  are given prior probability distributions in the Bayesian framework.

The standard Bayesian fPCA model (Crainiceanu and Goldsmith, 2010) assumes fPC scores to be independent draws from a univariate zero-centred normal distribution whose variance is dependent on the eigendimension  $k$ . The most straightforward hierarchical representation of the standard Bayesian fPCA model is

$$\begin{aligned}\tilde{Y}_{it} &= \sum_{k=1}^K \xi_{ik} \phi_{kt} + \epsilon_{it}, \\ \xi_{ik} | s_k &\sim \text{N}(0, s_k^{-1}), \\ \epsilon_{it} | \tau &\sim \text{N}(0, \tau^{-1}), \\ s_k &\sim \Gamma(a, b), \\ \tau &\sim \Gamma(a', b'),\end{aligned}\tag{3}$$

with  $a, a', b, b'$  usually set to low values (e.g.  $10^{-3}$ ). In this model the noise term is assumed to be Gaussian and independent gamma priors are placed over the precision parameters because of their conjugacy property, permitting closed-form conditional posterior distributions and the use of Gibbs sampling.

Recently, Liu et al. (2017) proposed to capture spatial dependence through a suitable model for the covariance of fPC scores. In particular, they defined  $\text{Cov}(\xi_{ik}, \xi_{i'k})$  as a function of the correlation coefficient  $\rho_{ii'k}$  which they modelled using the Matérn function family and estimating the relative parameters. This approach implies the a priori definition of a covariance structure which depends on the distance between observations; such assumptions might not be suitable for complex spatio-temporal phenomena such as brain activity where dependencies are the result of both structural and functional neuronal pathways as well of task-specific characteristics. In this study, we overcome these limitations to achieve a higher level of flexibility in the modelling of spatio-temporal covariance of neuroscientific data.

## 2.2 PCl-fPCA model

In this section we present the structure of the PCl-fPCA model and the features of this approach that improve the current methods for functional PCA. The following hierarchical model defines the probability distribution generating observed time series. We present and comment each level separately.

*Level 1:* As the standard Bayesian fPCA model in Equation (3), the distribution of the centred data given the parameters of the underlying smooth function and the noise term is given by:

$$\begin{aligned} \tilde{\mathbf{Y}}_i | \mathbf{X}_i, \tau &\sim N_T(\mathbf{X}_i, \tau^{-1}\mathbf{I}), \\ \mathbf{X}_i &= \sum_{k=1}^K \xi_{ik} \phi_k, \end{aligned} \quad (4)$$

where  $\tilde{\mathbf{Y}}_i$  and  $\mathbf{X}_i$  are  $T$ -dimensional vectors and  $N_T(\mathbf{X}_i, \tau^{-1}\mathbf{I})$  is the probability density function of a multivariate Gaussian random variable with mean  $\mathbf{X}_i$  and variance-covariance matrix  $\tau^{-1}\mathbf{I}$  such that  $\mathbf{I}$  denotes the  $T \times T$  identity matrix. Here we assume constant noise for simplicity although other characterisations are possible (Wang et al., 2016). It follows that the likelihood function is given by

$$L(\tilde{\mathbf{Y}} | \mathbf{X}, \tau) = \left(\frac{\tau}{2\pi}\right)^{Tn/2} \exp \left\{ -\frac{\tau}{2} \sum_{i=1}^n (\tilde{\mathbf{Y}}_i - \mathbf{X}_i)' (\tilde{\mathbf{Y}}_i - \mathbf{X}_i) \right\}. \quad (5)$$

*Level 2:* To encode fPC scores cluster membership we introduce a classification variable  $c_{ik}$  as a stochastic indicator that identifies which latent class  $j$  is associated with parameter  $\xi_{ik}$ . Prior distributions of the fPC scores  $\xi_{ik}$ , given the parameters of underlying clusters  $[(\mu_{1k}, s_{1k}), \dots, (\mu_{Jk}, s_{Jk})]$  and the classification variable  $c_{ik}$ , are given by

$$\xi_{ik} | c_{ik}, \mu_{1k}, \dots, \mu_{Jk}, s_{1k}, \dots, s_{Jk} \sim N(\mu_{c_{ik}}, s_{c_{ik}}^{-1}), \quad (6)$$

where  $\mu_{c_{ik}=j}$  and  $s_{c_{ik}=j}$  are mean and precision for the  $j$ -th cluster in the  $k$ -th eigendimension, respectively. Here we use a  $j$ -dimensional mixture of Gaussian distributions, independently

for each retained eigendimension  $k = 1, \dots, K$  as we permit different (independent) partitions for each mode of variation.

*Level 3:* Prior distributions for  $[(\mu_{1k}, s_{1k}), \dots, (\mu_{Jk}, s_{Jk})]$  and  $(c_{1k}, \dots, c_{nk})$ , given hyperparameters  $r_k, \beta_k$  and parameters  $(p_{1k}, \dots, p_{Jk})$ , are given by

$$c_{ik}|p_{1k}, \dots, p_{Jk} \sim f_C(p_{1k}, \dots, p_{Jk}), \quad (7)$$

$$\mu_{jk}|r \sim N(0, r_k^{-1}),$$

$$s_{jk}|\beta \sim \Gamma(1, \beta_k),$$

where  $f_C$  is the probability mass function of a categorical random variable which is the generalisation of a Bernoulli random variable to  $J$  outcomes. Cluster precision  $s_{jk}$  can be modelled also by using Uniform distributions on the cluster standard deviation where  $\sigma_{jk} = 1/\sqrt{(s_{jk})}$  (Gelman, 2006).

Hyperparameters  $r$  and  $\beta$  are often centred around empirical estimates in the literature (Richardson and Green, 1997); here, we take advantage of the properties of fPCA decomposition to tune the higher hierarchical levels in our model around weakly informative prior distributions. It follows from the Karhunen-Loève representation that, for any given  $i$ ,  $\xi_{ik}$  are uncorrelated fPC scores with monotonically decreasing variance given by the eigenvalues  $\lambda_k$  (Liu et al., 2017); therefore, sensible functions of the empirical estimates of the eigenvalues  $\hat{\lambda}_k$  can be used to fix  $r$  and  $\beta$  under the assumption that, for every eigendimension  $k$ , the position and dispersion of a cluster are both functions of  $\hat{\lambda}_k$ . We note that setting  $r = 1/\hat{\lambda}_k$  and  $\beta = \hat{\lambda}_k$  appeared to work well in our simulations and application.

*Level 4 and 5:* Prior distribution for  $(p_{1k}, \dots, p_{Jk})$ , given hyperparameter  $\alpha$  and prior distri-

bution for  $\alpha$  are given by

$$\begin{aligned} p'_{jk} | \alpha_k &\sim \text{Beta}(1, \alpha_k), \\ p_{1k} &= \frac{p'_{1k}}{\sum_{j=1}^J p'_{jk}}; \quad p_{jk} = \frac{p'_{jk} \prod_{l < j} (1 - p_{lk})}{\sum_{j=1}^J p'_{jk}}, \\ \alpha_k &\sim \text{U}[0, Q_k], \end{aligned} \tag{8}$$

where  $p_{jk}$  follow the stick-breaking construction (Sethuraman, 1994) with parameter  $\alpha_k$  modelling the prior belief over the mixing proportions  $p_{1k}, \dots, p_{Jk}$ . The dispersion parameter  $\alpha$  is usually fixed or modelled with a prior distribution; here we used the uniform distribution with a sufficiently large  $Q$  (Rasmussen, 2000; Medvedovic and Sivaganesan, 2002; Medvedovic et al., 2004; De Iorio et al., 2018).

Different tuning of  $s_{jk}$  and  $Q$  can be employed for  $k = 1$  and  $k = 2, \dots, K$  to incorporate the knowledge that the first eigendimension is more likely to capture global patterns in the data while the following dimensions are more sensitive to local features. For example, in the first eigendimension one can use the gamma distribution for the cluster precision in Equation 7 as it assigns more weights to large clusters than a uniform on the standard deviation which can be used instead in the subsequent dimensions. We provide specific examples in Section 3.1 and the results of a sensitivity analysis on  $Q, \beta$  and  $s$  in Web Appendix A.

The model structure can be displayed with a direct acyclic graph (DAG) (Web Appendix B, Figure 5). As  $J$  approaches infinity the model corresponds to a DP mixture model (Rasmussen, 2000; Neal, 2000; Medvedovic and Sivaganesan, 2002; Medvedovic et al., 2004; McDowell et al., 2018) with the difference that we have placed here multiple independent mixtures over the prior distribution of the fPC scores. In practice we used the truncated stick-breaking construction and tested the model with different values of  $J$ . All the conditional posteriors of this model (most of them available in closed form) are provided in Web Appendix C. Markov Chain Monte Carlo (MCMC) techniques are used to simulate from the joint posterior distribution of all parameters given the data. Reconstruction of the smooth



trajectories  $x_{it}$  is made easy by its linear relationship with the model parameters  $\xi_{ik}$ ; thus it is possible to obtain the posterior distribution of the  $i$ -th curve for every  $t$  and at every MCMC iteration  $w$ ,

$$x_{it}^{(w)} = \bar{x}_t + \sum_{k=1}^K \xi_{ik}^{(w)} \phi_{kt}, \quad i = 1, \dots, n; \quad t = 1, \dots, T, \quad (9)$$

where  $\bar{x}_t$  is the smoothed estimate of the sample mean. It follows that symmetric 95% point-wise credible intervals for each trajectory-specific mean can be obtained easily from Equation 9 by considering the  $(1 - \alpha)/2$  and  $\alpha/2$  quantiles of the  $x_{it}^{(w)}$  empirical distribution.

### 2.3 Clustering

In this section we focus on the clustering of fPC scores. DP mixture models implicitly produce classification through the allocation of each data point to a generating distribution with some probability. Clustering uncertainty can be evaluated at different levels such as the number of clusters, the size of each cluster and the observations (or parameters) assigned to them. Although a single partition is often of interest in applications, we note that exploring the cluster uncertainty can result in a better interpretation of the findings. In order to explore cluster uncertainty, we employ the empirical distribution of generated clusterings which can be considered a good approximation of the true posterior distribution after  $B$  burn-in iterations (Neal, 2000). We use functions of  $(\mathbf{c}_k^B, \mathbf{c}_k^{B+1}, \dots, \mathbf{c}_k^W)$  to obtain other distributions of interest, such as the number and size of clusters, as well as to compute Maximum a Posteriori Probabilities (MAPs) and pairwise probability matrices. MAPs are commonly used to identify the most probable clustering for each observation while  $i \times i'$  pair-wise probability matrices represent the posterior belief for all pair of curves to belong to the same cluster (Medvedovic and Sivaganesan, 2002; Medvedovic et al., 2004; McDowell et al., 2018).

Each of these distributions has some limitations. Simply considering the number of clusters does not account for size and stability (i.e. the number of times a cluster appears in the MCMC chain); however, we find it useful to test the presence of more than one cluster using

the Bayes factor. The size of clusters informs on the most relevant groups, though it does not guarantee that the observations joining a cluster remain loyal to it. In addition, MAPs are known to be limited by the possible presence of multiple modes and cases where individuals who share the same modal group are less frequently together than with others in different clusters. These issues can be addressed by the pairwise probability matrices but they can be hard to interpret, especially for large  $n$  and high cluster uncertainty.

Although we find each analysis by itself inadequate to draw robust conclusions, considering them together as a whole provides rich information on the (a posteriori) most likely partition for each eigendimension. We present an application of these analyses to fMRI data in Section 4.

#### *2.4 fPC score clustering as generalisation of standard clustering*

In the standard infinite mixture model based clustering, the indicators  $c_i = c_{i'} = j$  with  $i \neq i'$  would associate a couple of trajectories to a certain cluster  $j$  with probability  $P_{ii'}$ . On the other hand, by placing infinite mixtures over the fPC scores for every eigendimension retained, we allow for a more complex network of dependence among curves. In our model,  $c_{ik}$  and  $c_{i'k}$  would associate fPC scores  $i$  and  $i'$  to potentially different clusters in every eigendimension  $k$  with probability  $P_{ii'k}$ . It follows that a pair of curves could happen to share the same cluster in only part of the  $K$  eigendimension retained, expanding the standard model based clustering to a richer classification method. Furthermore, as each dimension represents a mode of variation (eigenfunction) and its importance (eigenvalue), our method offers additional insights into the underlying spatio-temporal structure of the data. In the following sections we show how clustering fPC scores produces a rich spatio-temporal exploration of complex neuroscientific data.

### 3. Simulation study

#### 3.1 *Simulation scenarios*

We performed a Monte Carlo (MC) simulation study to assess the performance of PCl-fPCA model and compare it to the standard Bayesian fPCA model in terms of both curves reconstruction and classification for different data generating processes and noise levels. We also included for comparison two frequentist approaches: the standard fPCA model (Ramsay and Silverman, 2005) and a modified version of the model by Liu et al. (2017) that we adapted to the features of neuroscientific data. In this latter model, curve dependence is captured through the fPC scores by means of independent Matérn functions for each eigendimension retained.

In order to test model performance with simulated data matching those of the targeted neuroscientific applications as closely as possible, we generated two eigenfunctions from simulated data resembling evoked responses in the brain. Subsequently, we defined three Data Generating Processes (DGP) that differ in the way the fPC scores are generated: in the first DGP (DGP1), scores are generated from different mixtures of Gaussian distributions in the two eigendimensions considered; in the second DGP (DGP2), fPC scores dependence in the first eigendimension is generated from a Matérn function while in the third DGP (DGP3), dependence of fPC scores is generated by independent Matérn covariance functions with different parameter values in each eigendimension.

We applied a random Gaussian noise and tested the models with both high and low signal-to-noise ratios (STN=6 and 1 respectively). Figure 1 shows an example from the set of 100 generated curves in DGP1 where either a low or high random noise is added.

[Figure 1 about here.]

One hundred datasets ( $L = 100$ ) for each DGP and STN were input to fPCA first for curve smoothing using cubic B-splines and dimension reduction by estimating the respective

eigenvalues and eigenfunctions. We retained a number of dimensions  $K$  explaining at least 95% of the total variability in curves. Figure 1 shows eigenfunctions and their weights extracted after smoothing a set of low-noise curves for the first DGP.

We adapted the general model presented in Section 2.2 to the specific simulation analysis using eigenvalues  $\lambda_k$  and their properties to develop vaguely informative prior distributions for the parameters  $r$ ,  $\beta$  and  $Q$  (Equations (7) and (8)) in the two eigendimensions retained  $k = 1, 2$ . We set  $r = (1/\hat{\lambda}_1, 1/\hat{\lambda}_2)$  and  $Q = (10, 5)$  as well as setting  $s_{j,1} \sim \Gamma(1, \lambda_1)$  and  $\sigma_{j,2} \sim U[0, \sqrt{\lambda_2}]$ . We made sure that even the smallest upper-bound  $Q$  of the dispersion parameter  $\alpha$  distribution represented an expected number of clusters a priori far higher than the ground truth (Escobar, 1994; Jara et al., 2007). A similar choice for  $\alpha$  was specified by De Iorio et al. (2018) due to the resulting stable computations.

We used Integrated Mean Square Error (IMSE) to measure and compare reconstruction performance between PCI-fPCA model and the competitor models. IMSE and its associated MC approximation for every curve  $i$  are given by

$$\text{IMSE}_i = \mathbb{E} \left\{ \int [\hat{x}_{it} - x_{it}]^2 dt \right\} \approx \frac{1}{L} \sum_{l=1}^L \left\{ \frac{1}{T} \sum_{t=1}^T (\hat{x}_{it} - x_{it})^2 \right\}, \quad (10)$$

where the expectation is taken with respect to the underlying curve  $x_i$ . The IMSE is a useful measure of performance in density estimation and is frequently used in curves reconstruction (Gentle, 2009; Rasheed and Aref, 2016). In addition, as curves correlation  $\rho_{ii'}$  is often of interest in neuroscientific applications (e.g. for measuring the degree of functional connectivity between brain areas), we measured correlations reconstruction using the L2 norm  $\|\hat{\rho}_{ii'} - \rho_{ii'}\|_2$  and compared it with those of the competitor models.

In order to assess the proposed model clustering performance in DGP1, we adopted the Adjusted Rand Index (ARI) to quantify the similarity between the estimated partitions (using MAP) and the ground truth for every MC dataset  $l$  and eigendimension  $k$ . The ARI is commonly used in the literature to assess clustering performance as it varies between exact

partition agreement (1) and when partitions agree no more than is expected by chance (0) (McDowell et al., 2018; Hubert and Arabie, 1985). Moreover, we measured the improvement in distance (L2 norm) between the posterior pair-wise probability matrices and the ground truth to evaluate the clustering performance of PCI-fPCA model by taking into account cluster uncertainty. Further details on the simulations setting can be found in Web Appendix D.

### 3.2 *Simulation results*

Results of curve and correlation reconstruction are reported in Figure 2.

[Figure 2 about here.]

The case where  $STN = 1$  is particularly relevant because neuroscientific data are usually affected by high noise. In this scenario, PCI-fPCA model highly improved curve reconstruction compared to all competitor models as 100% of the true curves were better recovered under PCI-fPCA and the median improvement in IMSE ranged from 22% to 45%. Moreover, a similar improvement was also obtained for DGP2 where clustering is present in only one eigendimension (Figure 2, bottom left). In addition, correlation reconstruction was also better achieved under PCI-fPCA with a median percentage of improvement ranging from 20% to 30% for DGP1 and 2% to 8% for DGP2 (Figure 2, right column). In the case of low noise ( $STN6$ ), the proposed model still performed better than the competitors for DGP1 and achieved values of IMSE and RMSE similar to those of the best competitor models in DGP2 (Web Appendix B, Figure 6).

Interestingly, even when no clusters are expected in both eigendimensions (DGP3), the performance of the PCI-fPCA was still comparable to the best ones achieved by competitor models for both low and high noise levels (Web Appendix B, Figure 7).

The performance of the PCI-fPCA model in terms of classification is reported in Table 1.

[Table 1 about here.]

The proposed model scored high in the ARI classification index in both eigendimensions studied; two and three clusters were expected in the first and second dimension respectively in DGP1. Clusters in the first eigendimension were always correctly identified by ARI for both high and low signal to noise ratios. The identification of three clusters in the second eigendimension was more challenging as they were smaller and nearer to each other; however, scores near 1 were almost always obtained when the low noise scenario was tested and even in the case of high noise we observed fairly high scores. Similar results were achieved by measuring the improvement in distance (L2 norm) between the posterior pairwise probability matrices and the ground truth to account for cluster uncertainty in the classification performance (Web Appendix D, Table 3).

Figure 8 in Web Appendix B provides evidence of the improved level of information achieved by PCI-fPCA in the DGP1 scenario.

Overall, PCI-fPCA model outperformed the competitors in curve reconstruction under different data generating processes, especially in the case of high noise in the data; moreover, for the case where clusters are not limited to one eigendimension, the proposed model was able to retrieve the original spatial partition in each eigendimension and bring to light important relationships between clusters. These results could further help the understanding of underlying neuroscientific phenomena in a real data scenario.

## 4. Application

### 4.1 fMRI setting

The study relates to a thirty-year-old healthy woman volunteer who underwent a resting-state fMRI at the Department of Radiology, Scientific Institute Santa Maria Nascente, Don Gnocchi Foundation (Milan, Italy) during February 2015. The recording was carried out

using a 1.5 T Siemens Magnetom Avanto (Erlangen, Germany) MRI scanner with 8-channel head coil. The subject was asked to lie down in the MRI machine in supine position with eyes closed while Blood Oxygenation Level Dependent Echo Planar Imaging (BOLD EPI) images were acquired. She was instructed to keep alert and relaxed; no specific mental task was requested.

High resolution T1-weighted 3D scans were also collected to be employed as anatomical references for fMRI data analysis. Standard pre-processing involved the following steps: motion and EPI distortion corrections, non-brain tissues removal, high-pass temporal filtering (cut-off 0.01 Hz) and artefacts removal using the FMRIB ICA-based Xnoiseifier (FIX) toolbox (Griffanti et al., 2014).

After the pre-processing, the resulting 4D dataset was aligned to the subject's high-resolution T1-weighted image, registered to MNI152 standard space and resampled to  $2 \times 2 \times 2 \text{ mm}^3$  resolution. One minute length series (sampled at 0.5 Hz) were extracted as the average signal within each of 90 regions of interest (ROIs) according to the Automated Anatomical Labeling (AAL90) coordinates. The resulting  $30 \times 90$  dataset was input to fPCA for curve smoothing and dimension reduction. The set of 90 smooth curves and the retained eigendimensions are shown in Figure 9 of Web Appendix B. We kept the first three dimensions explaining more than 85% of the total variability while accounting for more than 10% each.

We adapted the general model in Section 2.2 following the approach taken in the simulation study (Section 3.1), favouring global patterns in the first eigendimension and local patterns in the remaining dimensions. Furthermore, we carried out a sensitivity analysis by varying the values of the hyperparameters  $\beta, Q$  and the distribution of  $s$  in each dimension (Web Appendix A).

## 4.2 fMRI analysis results

The posterior probabilities associated with the single cluster (i.e. no clusters) scenario were 0.012, 0.124 and 0.058 for the three eigendimensions  $k$ , respectively. The Bayes factors (BF) for the first eigendimension was 0.53, which indicates some evidence against no clusters. Conversely, the second and third dimensions returned  $\text{BF} = 2.93$  and  $1.33$  respectively, which can be interpreted as evidence in favour of a single cluster. It is worth noting that, as the implied prior probabilities were highly in support of multiple clusters, the BF for  $k = 2$  and  $3$  show a diametrical change from prior to posterior belief.

Figure 3 shows the posterior probability for a cluster being empty and the posterior distributions of cluster size given it is not empty.

[Figure 3 about here.]

Two to three clusters seem to emerge in dimension 1; the size of the second cluster (Cl2, second from the right in Figure 3, bottom-left panel) has a peak around 20%, very small mass near zero, and a very low probability of being empty. The third cluster (Cl3) has a size peaking at 12% but more mass near zero and a higher probability of being empty. On the other hand, dimension 2 and 3 seem to suggest the presence of no more than one cluster each. The second cluster in both these dimensions has higher probability of being empty and the distributions of size have much more mass around zero. Furthermore, the distributions of the first cluster (Cl1) in both dimensions have a notable peak around 90% suggesting that, even when more than one cluster is considered, the large majority of fPC scores in dimension 2 and 3 tends to be gathered within a single large cluster.

The use of MAPs suggests there might be no more than 2 groups in the first dimension and 1 group in the second and third dimensions. Clustering with MAPs in the first dimension identified 9% of curves whose trajectories are wigglier and with a visibly shorter inter-peak difference between the first positive and negative peaks compared to the other group



(Web Appendix B, Figure 10). Figure 11 of Web Appendix B shows an example of curve reconstruction using the posterior mean and 95% point-wise credible bands of the subject specific mean. Curves in cluster 2 pertain to brain areas from the occipital lobe (Calcarine, Cuneus, Lingual, Inferior Occipital Gyrus) and parietal lobe (Precuneus).

By analysing the pairwise probability matrix, a more comprehensive classification emerged. The previously dichotomous partition in dimension  $k = 1$  is now enriched by a third group of brain areas with no clear clustering preference (grey band at the top-right of the pairwise probability matrix in Figure 4).

[Figure 4 about here.]

Cluster 2 comprises 16% of curves which all represent areas from the occipital lobe (yellow-light dots), while curves in cluster 3 (blue-dark dots) belong to the cingulate cortex (Middle and Posterior Cingulate Cortex), parietal (Parietal Superior Lobule, Precuneus) and temporal (Middle and Inferior Temporal Gyrus) lobes (Figure 4, a color version of this figure can be found in the online version of the article).

We note that these three clusters are supported in the neuroimaging literature. It is well established that primary and extra-striate visual regions are active at rest (Van Den Heuvel and Pol, 2010) and have a role in processing mental imagery (Zhang et al., 2018). Just outside the visual cortex, The Temporal Inferior Gyrus takes part to the visual ventral stream which links information from the visual cortex to memory and recognition (Milner, 2017). Moreover, the Posterior Cingulate Cortex is known to interact with several different brain networks simultaneously and it participates in the Default Mode Network together with part of the parietal lobe (Leech et al., 2012). Conversely, it has been suggested that areas pertain to the Prefrontal Cortex (all included in cluster 1) have less long-range connectivity in the resting state condition (Tomasi and Volkow, 2011).

Finally, the sensitivity analysis further confirmed our findings as they were robust to changes in both shape and value of the hyperparameters (Web Appendix A).

## 5. Discussion

The processing of the human brain is a complex phenomenon in both time and space. The modelling of spatio-temporal datasets in the big data era is a challenge becoming every day more demanding as we struggle to keep up with the overwhelmingly larger datasets we are required to make sense of. Moreover, the extraordinary advancements in neuroimaging of the last decades have focused large part of neuroscientists' efforts on the spatial domain both in clinical practice and research. Nonetheless, the time domain retains important neurophysiological information on brain functioning and neuronal health and without it we are at risk of drawing partial and possibly wrong conclusions on how the brain works.

In the present study we proposed a model that combines functional PCA and Bayesian nonparametric techniques to explore spatio-temporal datasets flexibly. We combined the interesting idea of introducing spatial dependence among curves through the fPC scores proposed by Liu et al. (2017) with the infinite Gaussian mixture model (Rasmussen, 2000; Medvedovic and Sivaganesan, 2002; Medvedovic et al., 2004; McDowell et al., 2018) to obtain a flexible modelling of the covariance structure. The main results show a clear superiority of the PCI-fPCA model both in curve and correlation reconstruction compared to different state-of-the-art fPCA models, particularly in the presence of high noise (as it is often the case in brain recordings) and the ability of exploring curves dependence dynamically allowing for different spatial patterns for each eigendimension retained.

Improvements in the reconstruction of high-noise corrupted curves were also reported by Liu et al. (2017); in fact, the beneficial effect of accounting for curves similarity is more evident when the true signal is well masked behind the noise. Nevertheless, a direct modelling of large covariance matrices often resorts to the use of common covariance functions to avoid

overparametrisation. The use of functions such as Matérn or rational quadratic implies a priori knowledge on the shape of spatial dependence. We believe that this approach does not suit highly complex phenomena, such as brain processing, where dependence has a much more elaborate architecture than a simple function of spatial proximity. Clustering the fPC scores allowed us to capture dependence among curve flexibly without the need to estimate the relative spatial covariance matrix. Interestingly, our results suggest that the high flexibility of PCl-fPCA model makes it a very suitable choice even in the cases where a single or even none of the eigendimensions retained support clustering of fCP scores.

DP mixture models have been also used for clustering time series through the clustering of the relative coefficients in a basis expansion representation (Angelini et al., 2012; James and Sugar, 2003; Ray and Mallick, 2006; Zhou and Wakefield, 2006). In the present study we moved from a global clustering of the data to a local clustering of fPC scores to address both the exploration of brain activity data and to improve curve reconstruction. This approach offers a richer classification technique as curves can potentially be assigned to different clusters in each eigendimension and a different number of clusters in every eigendimension is allowed. It follows that the assumption of separability of the cross-covariance matrix is avoided and rich time-space interactions can be captured by the model; as a consequence, this local borrowing of information also improves the reconstruction of the underlying smooth process. In addition, we benefit from the properties of the fPCA expansion to tune the hyperparameters and improve the MCMC convergence.

Cross-covariance matrices are often intractable if we do not resort to compromises in our models. A sensible compromise should be tailored to the type of specific data. In this study, we compromised with the time domain by using fPCA with a fixed number of eigendimensions while giving flexibility in the modelling of spatial dependence. This

served the purpose of breaking off from the separability assumption while, at the same time, favouring interpretation and a simple model structure.

By means of a simulation study and the analysis of an fMRI dataset we demonstrate that PCl-fPCA is effective in recovering the underlying smooth curves and it produces a valuable exploration of the spatio-temporal dependence in brain time series.

It is worth noting that, although we obtained more than one cluster only in the first eigendimension of our resting-state fMRI data, we found this partition in line with the current neuroscientific literature and we showed that PCl-fPCA achieved the best performance in terms of curve and correlation reconstruction even in this scenario. Moreover, we expect more evident clustering behaviours of curves to be found in task-based experiments where specifically designed tasks enhance neuronal synchronisation of different brain areas at different time points. Therefore, in our future work we plan to investigate such scenarios and expand our approach to replicated data and multiple subjects experiments. Exploring inter-individual patterns of functional connectivity and their uncertainty can help answer important questions not only in the study of brain processes but also in the characterisation, early diagnosis and prognosis of brain diseases.

#### ACKNOWLEDGEMENTS

fMRI data were kindly provided by IRCCS Santa Maria Nascente, Don Carlo Gnocchi foundation of Milan (Italy).

#### REFERENCES

Angelini, C., De Canditiis, D., and Pensky, M. (2012). Clustering time-course microarray data using functional Bayesian infinite mixture model. *Journal of Applied Statistics* **39**, 129–149.

- Crainiceanu, C. M. and Goldsmith, A. J. (2010). Bayesian functional data analysis using WinBUGS. *Journal of Statistical Software* **32**,.
- De Iorio, M., Gallot, N., Valcarcel, B., and Wedderburn, L. (2018). A Bayesian semiparametric Markov regression model for juvenile dermatomyositis. *Statistics in Medicine* **37**, 1711–1731.
- Escobar, M. D. (1994). Estimating normal means with a Dirichlet process prior. *Journal of the American Statistical Association* **89**, 268–277.
- Escobar, M. D. and West, M. (1995). Bayesian density estimation and inference using mixtures. *Journal of the American Statistical Association* **90**, 577–588.
- Gelman, A. (2006). Prior distributions for variance parameters in hierarchical models (comment on article by Browne and Draper). *Bayesian Analysis* **1**, 515–534.
- Gelman, A., Stern, H. S., Carlin, J. B., Dunson, D. B., Vehtari, A., and Rubin, D. B. (2013). *Bayesian Data Analysis*. Chapman and Hall/CRC, 3rd edition.
- Gentle, J. E. (2009). *Computational Statistics*. Springer.
- Griffanti, L., Salimi-Khorshidi, G., Beckmann, C. F., Auerbach, E. J., Douaud, G., Sexton, C. E., Zsoldos, E., Ebmeier, K. P., Filippini, N., Mackay, C. E., et al. (2014). Ica-based artefact removal and accelerated fMRI acquisition for improved resting state network imaging. *Neuroimage* **95**, 232–247.
- Hasenstab, K., Scheffler, A., Telesca, D., Sugar, C. A., Jeste, S., DiStefano, C., and Şentürk, D. (2017). A multi-dimensional functional principal components analysis of EEG data. *Biometrics* **73**, 999–1009.
- Hubert, L. and Arabie, P. (1985). Comparing partitions. *Journal of Classification* **2**, 193–218.
- James, G. M. and Sugar, C. A. (2003). Clustering for sparsely sampled functional data. *Journal of the American Statistical Association* **98**, 397–408.
- Jara, A., García-Zattera, M. J., and Lesaffre, E. (2007). A Dirichlet process mixture model

- for the analysis of correlated binary responses. *Computational Statistics & Data Analysis* **51**, 5402–5415.
- Leech, R., Braga, R., and Sharp, D. J. (2012). Echoes of the brain within the posterior cingulate cortex. *Journal of Neuroscience* **32**, 215–222.
- Liu, C., Ray, S., and Hooker, G. (2017). Functional principal component analysis of spatially correlated data. *Statistics and Computing* **27**, 1639–1654.
- McDowell, I. C., Manandhar, D., Vockley, C. M., Schmid, A. K., Reddy, T. E., and Engelhardt, B. E. (2018). Clustering gene expression time series data using an infinite gaussian process mixture model. *PLoS Computational Biology* **14**, e1005896.
- Medvedovic, M. and Sivaganesan, S. (2002). Bayesian infinite mixture model based clustering of gene expression profiles. *Bioinformatics* **18**, 1194–1206.
- Medvedovic, M., Yeung, K. Y., and Bumgarner, R. E. (2004). Bayesian mixture model based clustering of replicated microarray data. *Bioinformatics* **20**, 1222–1232.
- Milner, A. (2017). How do the two visual streams interact with each other? *Experimental Brain Research* **235**, 1297–1308.
- Neal, R. M. (2000). Markov chain sampling methods for Dirichlet process mixture models. *Journal of Computational and Graphical Statistics* **9**, 249–265.
- Plummer, M. et al. (2003). Jags: A program for analysis of bayesian graphical models using gibbs sampling. In *Proceedings of the 3rd international workshop on distributed statistical computing*, volume 124, page 10. Vienna, Austria.
- Ramsay, J., Hooker, G., and Graves, S. (2009). *Functional Data Analysis with R and MATLAB*. Springer Science & Business Media.
- Ramsay, J. and Silverman, B. W. (2005). *Functional Data Analysis*. Springer Series in Statistics.
- Rasheed, H. A. and Aref, R. (2016). Bayesian inference for parameter and reliability function

- of inverse Rayleigh distribution under modified squared error loss function. *Australian Journal of Basic and Applied Sciences* **10**, 241–248.
- Rasmussen, C. E. (2000). The infinite Gaussian mixture model. In *Advances in neural information processing systems*, pages 554–560.
- Ray, S. and Mallick, B. (2006). Functional clustering by Bayesian wavelet methods. *Journal of the Royal Statistical Society: Series B (Statistical Methodology)* **68**, 305–332.
- Richardson, S. and Green, P. J. (1997). On Bayesian analysis of mixtures with an unknown number of components (with discussion). *Journal of the Royal Statistical Society: Series B (Statistical Methodology)* **59**, 731–792.
- Sethuraman, J. (1994). A constructive definition of Dirichlet priors. *Statistica sinica* pages 639–650.
- Sørensen, H., Goldsmith, J., and Sangalli, L. M. (2013). An introduction with medical applications to functional data analysis. *Statistics in Medicine* **32**, 5222–5240.
- Suarez, A. J., Ghosal, S., et al. (2017). Bayesian estimation of principal components for functional data. *Bayesian Analysis* **12**, 311–333.
- Tian, T. S. (2010). Functional data analysis in brain imaging studies. *Frontiers in Psychology* **1**, 35.
- Tomasi, D. and Volkow, N. D. (2011). Functional connectivity hubs in the human brain. *Neuroimage* **57**, 908–917.
- Van Den Heuvel, M. P. and Pol, H. E. H. (2010). Exploring the brain network: a review on resting-state fMRI functional connectivity. *European Neuropsychopharmacology* **20**, 519–534.
- Viviani, R., Grön, G., and Spitzer, M. (2005). Functional principal component analysis of fMRI data. *Human Brain Mapping* **24**, 109–129.
- Wang, J.-L., Chiou, J.-M., and Mueller, H.-G. (2016). Review of functional data analysis.

*Annual Review of Statistics and its Application* **3**, 257–295.

- Wolfson, O. (2018). Understanding the human brain via its spatio-temporal properties (vision paper). In *Proceedings of the 26th ACM SIGSPATIAL International Conference on Advances in Geographic Information Systems*, pages 85–88. ACM.
- Zhang, Z., Zhang, D., Wang, Z., Li, J., Lin, Y., Chang, S., Huang, R., and Liu, M. (2018). Intrinsic neural linkage between primary visual area and default mode network in human brain: evidence from visual mental imagery. *Neuroscience* **379**, 13–21.
- Zhou, C. and Wakefield, J. (2006). A Bayesian mixture model for partitioning gene expression data. *Biometrics* **62**, 515–525.

#### SUPPORTING INFORMATION

Web Appendix A, B, C and D are available with this paper at the Biometrics website on Wiley Online Library.

*Received October 2019. Revised —- —-. Accepted —- —-.*

#### APPENDIX

Please note that, upon publication, software in the form of R codes will be available from an online repository.

##### *Web Appendix A - Sensitivity analysis*

In the sensitivity analysis we tested how changing the prior expected number of clusters and cluster size impacted on our findings in the application on fMRI data of Section 4 (Table 2). Overall, our results are substantially robust to changes in the shape and value of the hyperparameters. For the first eigendimension we found only few curves transitioning from cluster 2 to cluster 1 as the prior size and number of clusters increase; vice versa, we found some of the curves with high classification uncertainty (see the analysis of pairwise



probabilities in Section 4.2) moving into cluster 2 as the prior size and number of clusters decrease. The other eigendimensions showed only 1 cluster each in every scenario tested.

[Table 2 about here.]

### *Web Appendix B - Additional figures*

Additional figures not shown in the paper that further clarify the features of our model, simulation study and application.

Figure 5 shows the Direct Acyclic Graph (DAG) representing the structure of the PCI-fPCA model.

Figure 6 and 7 report the result of the simulation study in the case of low noise (STN6) and Data Generating Process 3, where fPC scores correlations were generated by Matérn functions in each eigendimension. Figure 8 shows a possible way to read the (rich) results obtained with PCI-fPCA model.

Figure 9 presents the fMRI data used in the application and the relative eigendimensions retained. Figure 10 reports the (intermediate) results of the application of Maximum a Posteriori Probabilities (MAP) for clustering the fPC scores.

Figure 11 shows reconstructed fMRI curves from two different clusters and their credible bands.

[Figure 5 about here.]

[Figure 6 about here.]

[Figure 7 about here.]

[Figure 8 about here.]

[Figure 9 about here.]

[Figure 10 about here.]

[Figure 11 about here.]

### Web Appendix C - Posterior conditional distributions

In this section we present the posterior conditional distributions for the parameters of our model (Section 2.2).

$$\begin{aligned}
\xi_{ik}|y_{it}, c_{i,k}, \mu_{jk}, s_{jk}, \tau &\sim N\left(\frac{\tau \sum_{t=1}^T y_{it}\phi_{tk} + s_{jk}\mu_{jk}}{\tau + s_{jk}}, \frac{1}{\tau + s_{jk}}\right), \\
\tau|\tilde{\mathbf{y}}_1, \dots, \tilde{\mathbf{y}}_n, a', b' &\sim \Gamma\left(\frac{Tn}{2} + a', \frac{\sum_{i=1}^n \sum_{t=1}^T \left(\tilde{y}_{it} - \sum_{k=1}^K \xi_{ik}\phi_{kt}\right)^2}{2} + b'\right), \\
\mu_{jk}|\mathbf{c}_k, \boldsymbol{\xi}_k, s_{jk}, v_k, r_k &\sim N\left(\frac{s_{jk} \sum_{i:c_{ik}=j} \xi_{ik} + v_k r_k}{n_{jk}s_{jk} + r_k}, \frac{1}{n_{jk}s_{jk} + r_k}\right), \\
s_{jk}|\mathbf{c}_k, \boldsymbol{\xi}_k, \beta_k, z_k, \mu_{jk} &\sim \Gamma\left(\frac{n_{jk}}{2} + z_k, \frac{1}{2} \sum_{i:c_i=j}^{n_{jk}} (\xi_{ik} - \mu_{jk})^2 + \beta_k\right), \\
c_{ik}|\mathbf{p}_k, \boldsymbol{\xi}_k, \boldsymbol{\mu}_k, \mathbf{s}_k, \alpha_k &\propto \sum_{j=1}^J p_{jk} s_{jk}^{1/2} \exp\left\{\frac{-s_{jk}}{2} (\xi_{ik} - \mu_{jk})^2\right\}, \\
p_{1k} &= \frac{p'_{1k}}{\sum_{j=1}^J p'_{jk}}; \quad p_{jk} = \frac{p'_{jk} \prod_{l < j} (1 - p_{lk})}{\sum_{j=1}^J p'_{jk}}, \\
p'_{jk}|c_{ik}, \alpha_k &\sim \text{Beta}\left(n_{jk} + 1, \alpha_k + \sum_{l=j+1}^J n_{lk}\right), \\
\alpha_k|\mathbf{p}_k &\propto \alpha_k^J \exp\left\{\alpha_k \sum_{j=1}^J \log(1 - p'_{jk})\right\}; \quad \text{for } \mathcal{S}_{\alpha_k} = [0, U_k],
\end{aligned}$$

where  $n_{jk}$  are the fPC scores in the  $j^{\text{th}}$  cluster of the  $k^{\text{th}}$  eigendimension and  $\mathcal{S}_{\alpha_k}$  is the posterior support of  $\alpha_k$ .

In our model we fixed  $a' = b' = 10^{-3}$ ,  $z_k = 1$ ,  $v_k = 0$  and the upper-bound for the support of  $\alpha_k$  takes into account the dimension-specific features of functional PCA as detailed in the paper, Chapter 2.2.

### Web Appendix D - Simulation study setting

*Data Generating Process 1 (DGP1).* Two groups of curves (Group 1 and 2) of length  $T = 150$  time series for a total of  $n = 100$  curves were generated by using a mixture

of 2 normal distributions on the first eigendimension. Group 1 (red and orange curves in Figure 1 in the paper) was composed of 50 trajectories representing active brain areas, while Group 2 (blue curves) represented all other brain regions. Within Group 1, two different sub-patterns (red and orange curves) representing meaningful differences in the way brain areas are activated were obtained by a further partition of the curves into two clusters in the second eigendimension.

*Data Generating Process 2 (DGP2).* The mixture on the first eigendimension in DGP1 was replaced by a zero-centred multivariate normal distribution with covariance matrix defined by a Matérn function of the form

$$C_{1/2}(d) = \sigma^2 \exp\left\{\frac{-d}{\rho}\right\},$$

with  $\rho = 0.9$  and  $\sigma^2 = 10$ . The second eigendimension was characterised by a mixture of three normal distributions.

*Data Generating Process 3 (DGP3).* The mixtures in the first and second eigendimensions of DGP1 were replaced by multivariate normal distributions with covariance matrix defined by Matérn functions with parameters  $(\rho = 0.9, \sigma^2 = 10)$  and  $(\rho = 0.7, \sigma^2 = 5)$  respectively.

#### *Further details*

- For the Matérn model, we used the approach detailed in Liu et al. (2017, Section 3.2 and 3.3) to capture curve dependence. We employed and adapted the R codes provided by the authors in the on-line supplementary materials. However, we did not employ their cross-covariance local linear smoother and kept the same smoothing approach for all the different models tested.
- We coded the model in R using the `rjags` package (Plummer et al., 2003); we employed a conservative approach (Medvedovic and Sivaganesan, 2002; Gelman et al., 2013) using 100,000 iterations for the burn-in and retaining the subsequent 100,000 MCMC iterations.

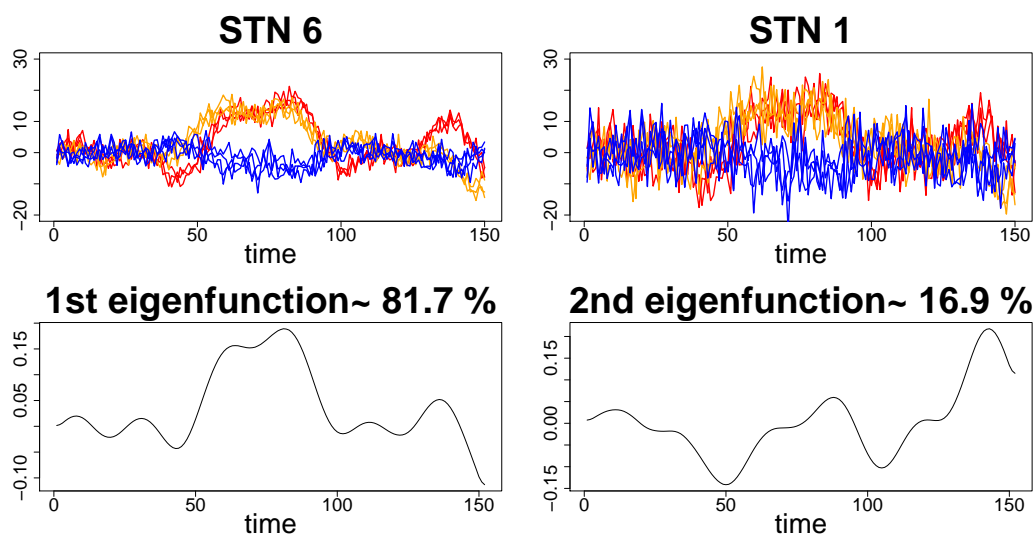
This ensured good convergence results for all the parameters of interest. We used a thinning of 5 to store results from 100 simulated datasets efficiently (approximately 70 MB each with  $K=2$ ). It takes 36 minutes on average (2.9 SD) to complete one simulation run on a 2-core Intel CPU running at 2.7 GHz.

- In order to evaluate the clustering performance of the PCl-fPCA model by taking into account cluster uncertainty we defined, for a given eigendimension  $k$ , a measure of distance between the true partition and the pairwise probability matrix which we compared with that of the standard Bayesian fPCA model (i.e. where no cluster is expected). We named the following formula Clustering Improvement Index (CII):

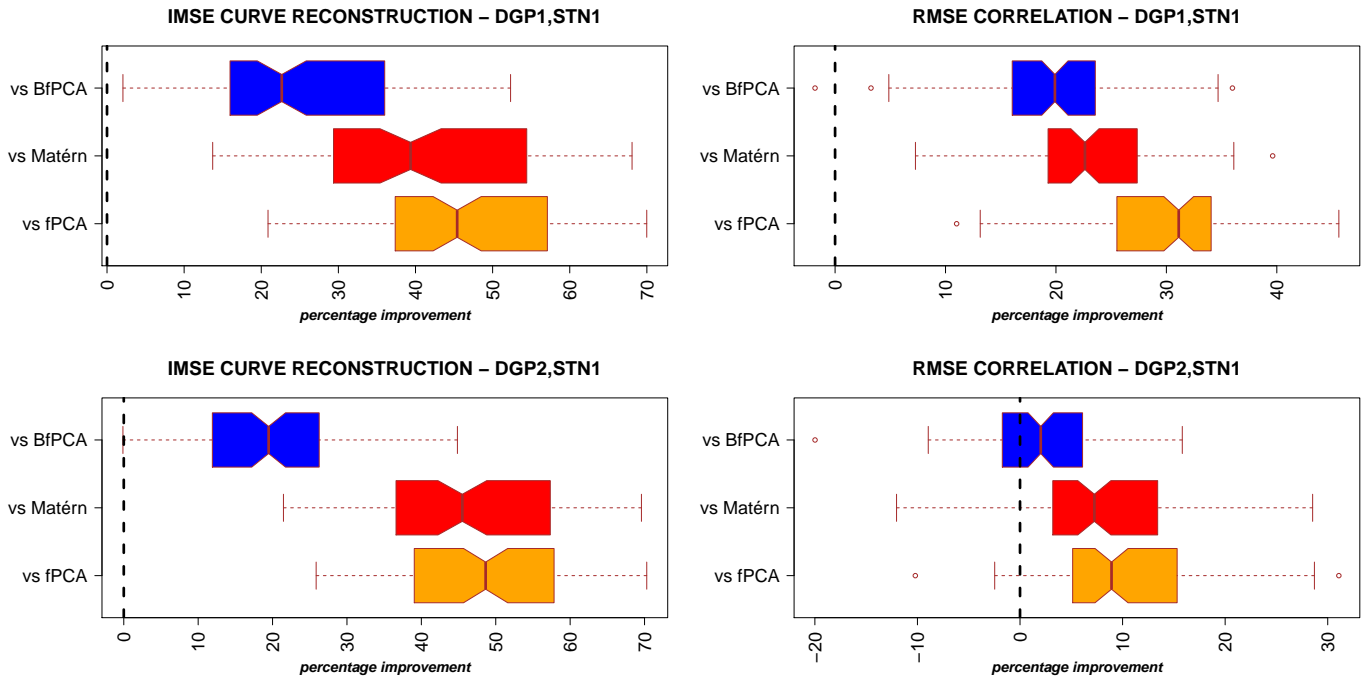
$$CII = \frac{\|M_{\text{std}} - G\|_2 - \|M_{\text{new}} - G\|_2}{\|M_{\text{std}} - G\|_2} \in \left[ \frac{\|M_{\text{std}} - G\|_2 - \|\bar{G} - G\|_2}{\|M_{\text{std}} - G\|_2}, 1 \right], \quad (\text{A.1})$$

where  $M$  are the clustering matrices for the two competing models (new and standard),  $G$  the underlying truth and  $\bar{G}$  the worst case-scenario we could incur with  $M_{\text{new}}$  (i.e. the case where the true 0s and 1s are inverted). It follows that CII is 1 (i.e. 100% improvement) when the clustering is completely accurate and values around 0 indicate no real advantage compared with the standard model. Results in Table 3 are in line with those obtained with ARI highlighting a good clustering performance of the proposed model in both eigendimensions studied for all Monte Carlo datasets.

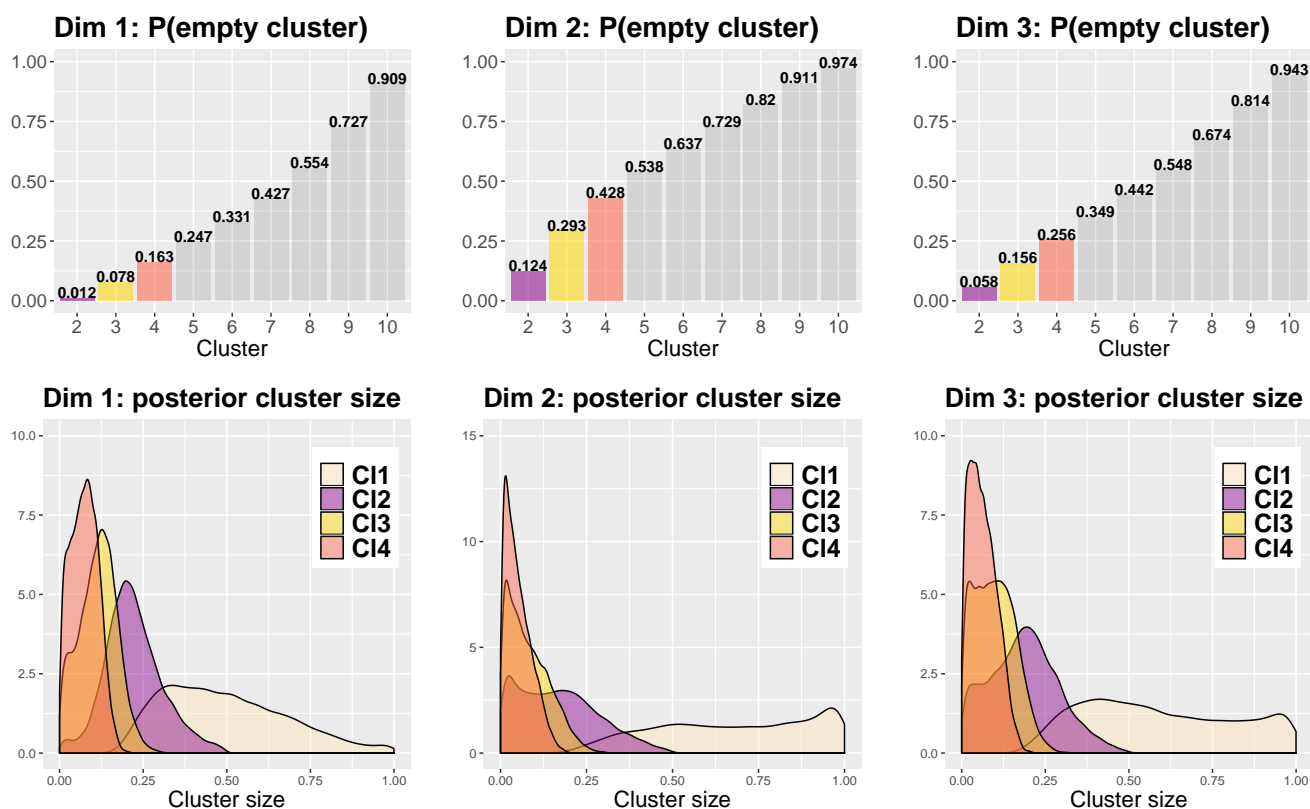
[Table 3 about here.]



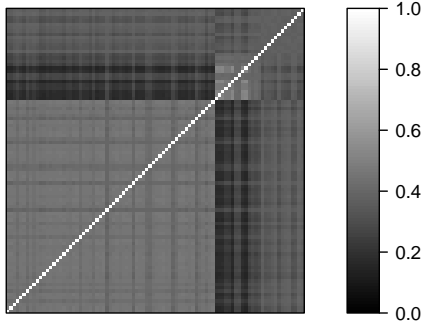
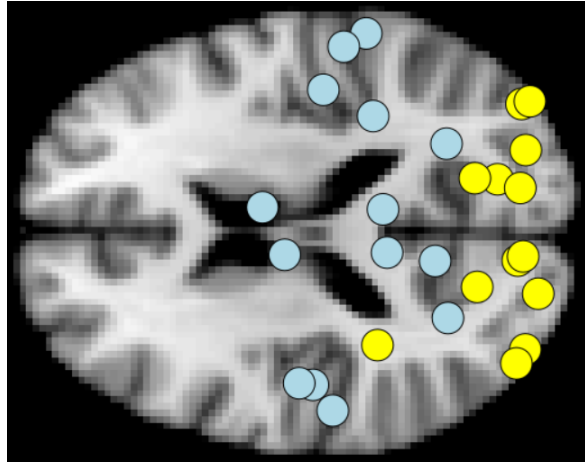
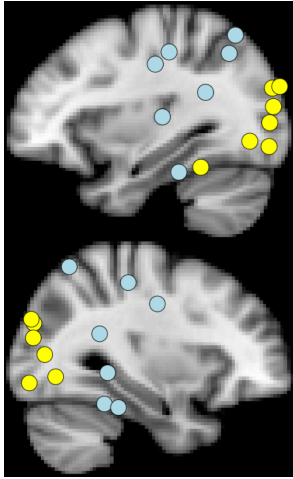
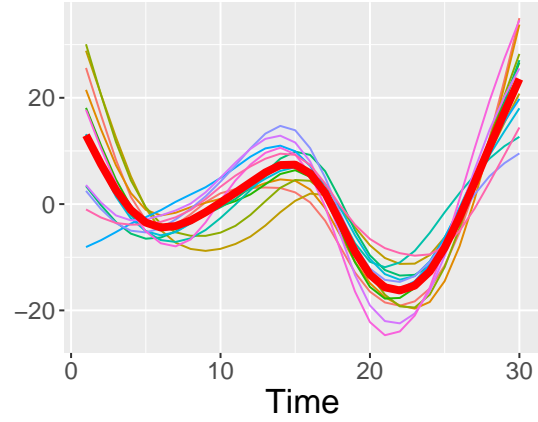
**Figure 1.** Simulation study: (Top) an example of curves from DGP1 with low random noise (STN6) and high random noise (STN1). (Bottom) the first and second eigenfunctions extracted from a set of DGP1 curves with STN6. This figure appears in color in the electronic version of this article.



**Figure 2.** Simulation study: curve and correlation reconstruction for Data Generating Processes (DGP) 1 and 2 with high noise (STN1). IMSE and RMSE improvement percentage using PCL-fPCA model versus standard Bayesian fPCA (BfPCA), fPCA model for correlated curves (Matérn) and standard fPCA model (fPCA). This figure appears in color in the electronic version of this article.



**Figure 3.** fMRI data analysis: cluster identification. The first row shows the posterior probabilities of being empty for the second to tenth clusters in the three eigendimensions (Dim 1:3) analysed. The second row shows the posterior distributions of cluster size (given it is not empty) among the first four clusters (C11:C14, right to left). This figure appears in color in the electronic version of this article.

**Pairwise probability matrix****Cluster 2 (1st dim)**

**Figure 4.** fMRI data analysis: cluster identification with pairwise probabilities. Top-left: pairwise probabilities suggesting a tripartition of curves in the first eigendimension. Top-right: cluster 2 updated according to the partition suggested by pairwise probabilities. The thick line represents the cluster mean. Bottom: the 3-D representation of clusters 2 and 3 over sagittal and axial slices of the human brain, where yellow (light) dots represent locations in cluster 2 and blue (dark) dots those in cluster 3. This figure appears in color in the electronic version of this article.



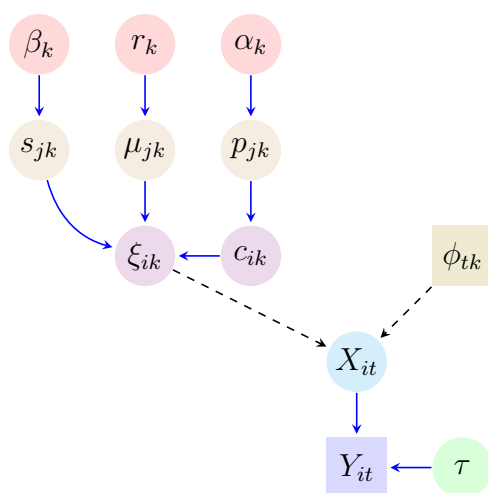


**Figure 5.** Parameters Clustering (PCI) fPCA model. Squares= observed random variables; circles= unobserved random variables; dashed= deterministic relationship; solid= stochastic relationship.

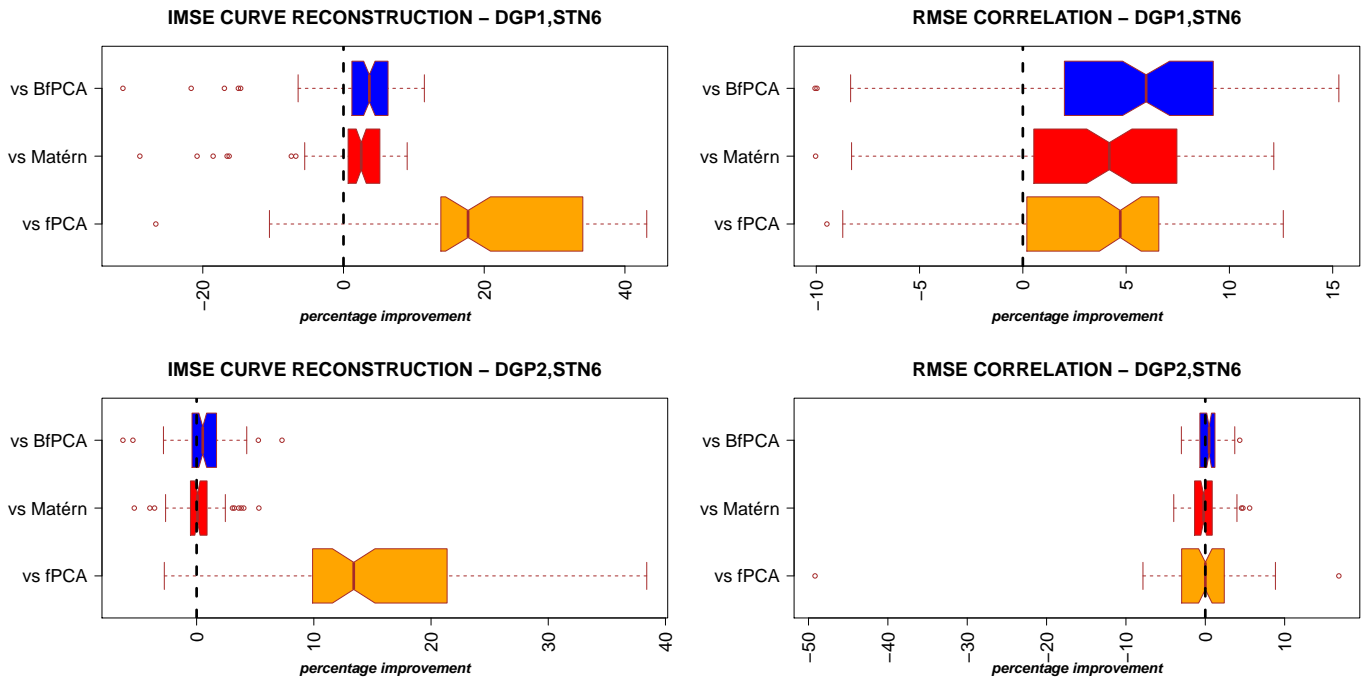


**Figure 6.** Simulation study: curve and correlation reconstruction for Data Generating Processes (DGP) 1 and 2 with low noise (STN6). IMSE and RMSE improvement percentage using PCL-fPCA model versus standard Bayesian fPCA (BfPCA), fPCA model for correlated curves (Matérn) and standard fPCA model (fPCA).

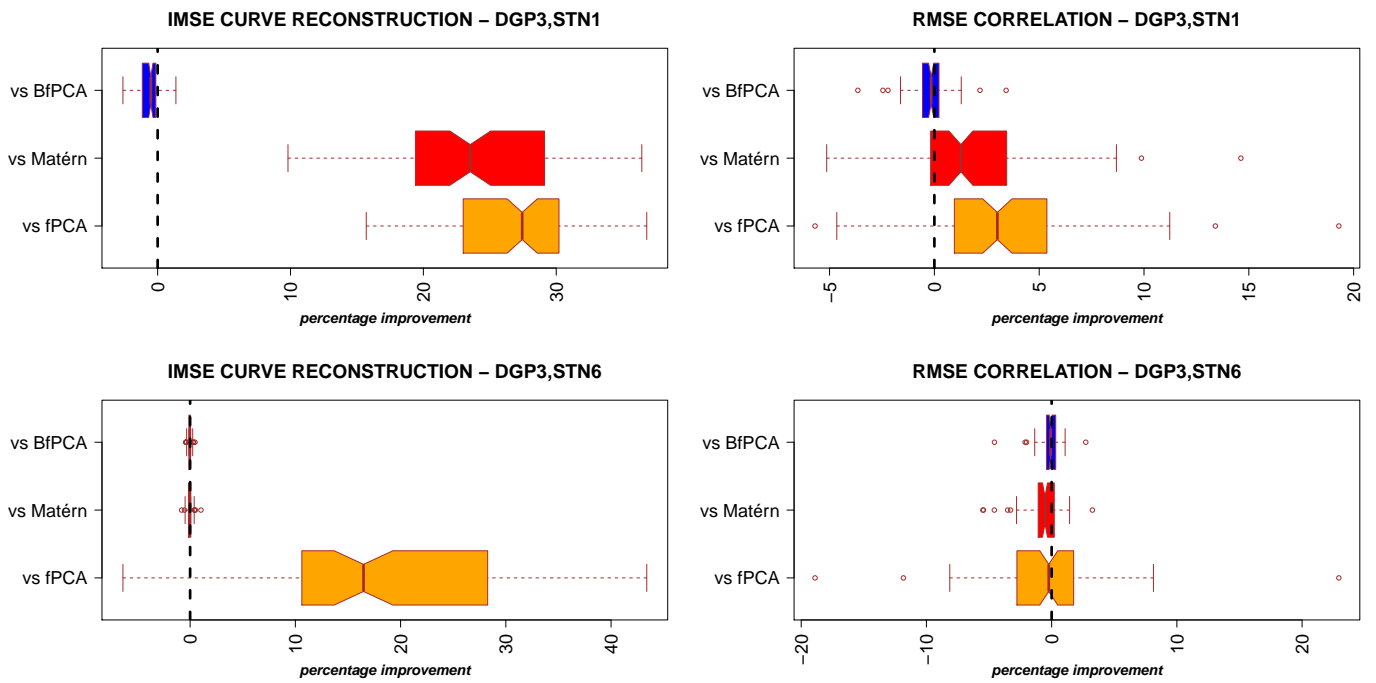


**Figure 7.** Simulation study: curve and correlation reconstruction for Data Generating Processes (DGP) 3 with high and low noise (STN1 and STN6, respectively). IMSE and RMSE improvement percentage using PCI-fPCA model versus standard Bayesian fPCA (BfPCA), fPCA model for correlated curves (Matérn) and standard fPCA model (fPCA).

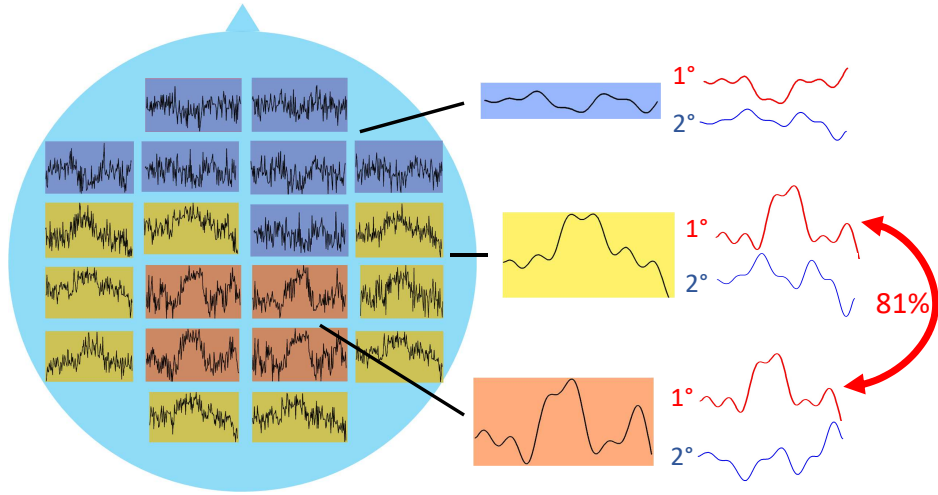


**Figure 8.** Simulation study - DGP1 scenario: from noise-corrupted time-series to spatio-temporal classified smooth curves. The figure exemplifies information obtained by using PCI-fPCA model. Among 100 noise-corrupted time-series, the model identified three spatial clusters; each group can be represented by the mean of the relative reconstructed curves and the two modes of variation which characterise it (red: 1st eigendimension, blue: 2nd). The new classification method brings to light a strong link (red arrow) between two clusters via the first eigendimension, explaining 81% of the variability in the data.

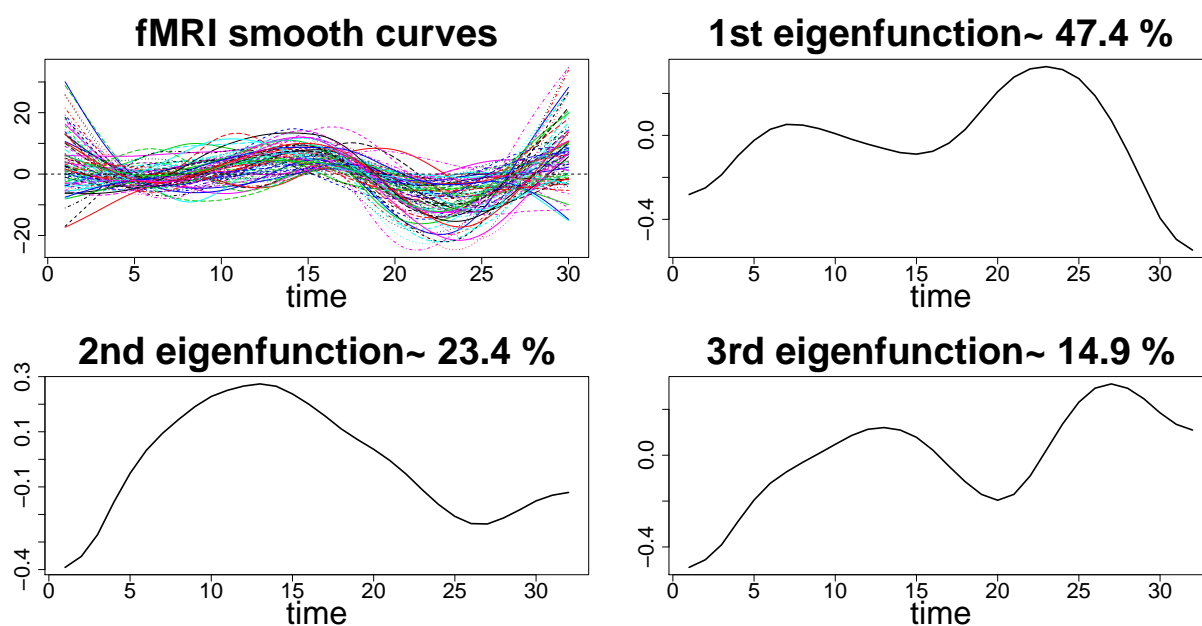


**Figure 9.** fMRI data analysis: fPCA decomposition. The dataset composed by 90 curves (after smoothing) and the three retained eigendimensions explaining 85% of the total variability in the curves.

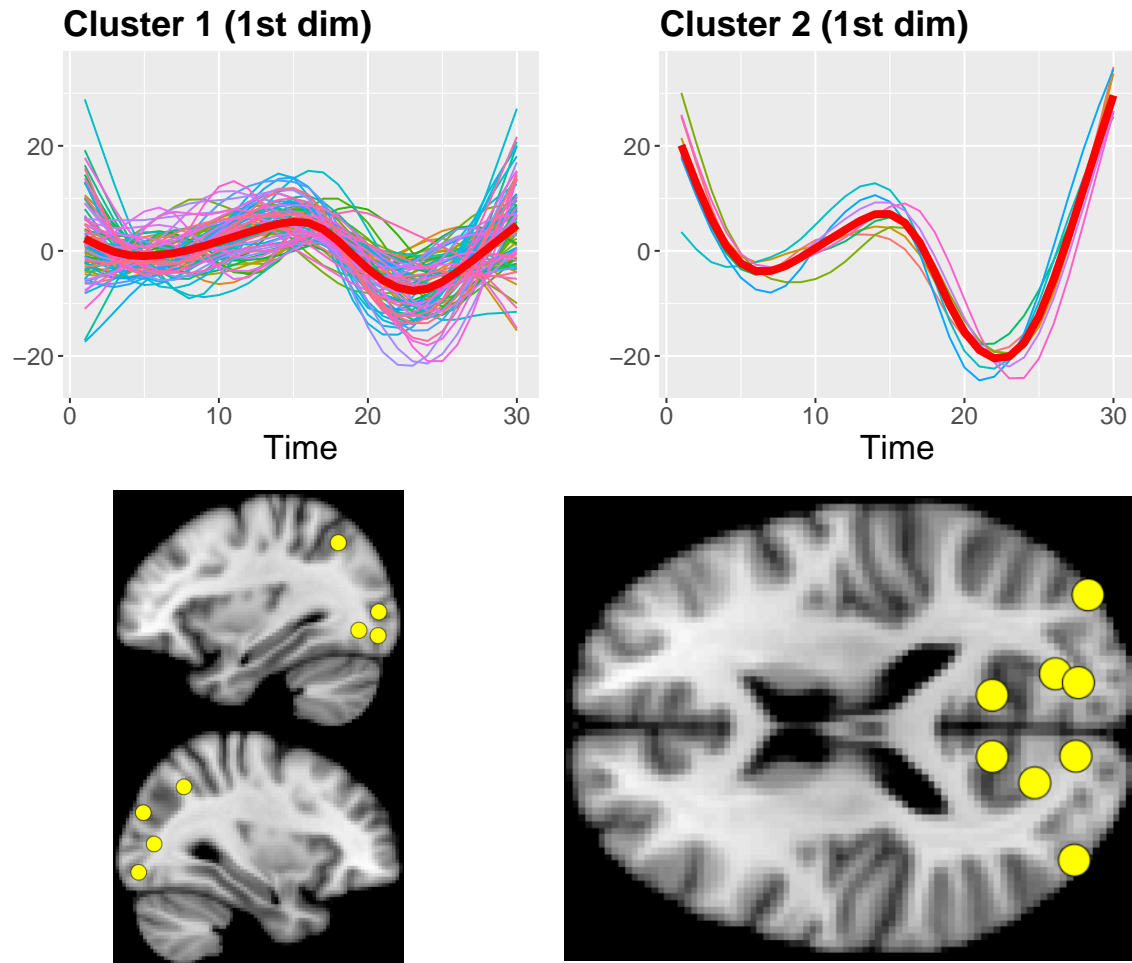


**Figure 10.** fMRI data analysis: cluster identification with MAPs. Top row: two clusters obtained in the first eigendimension together with the respective overall means (thick line). Bottom row: 3D localisation of cluster 2 (yellow dots) over sagittal and axial slices of human brain.

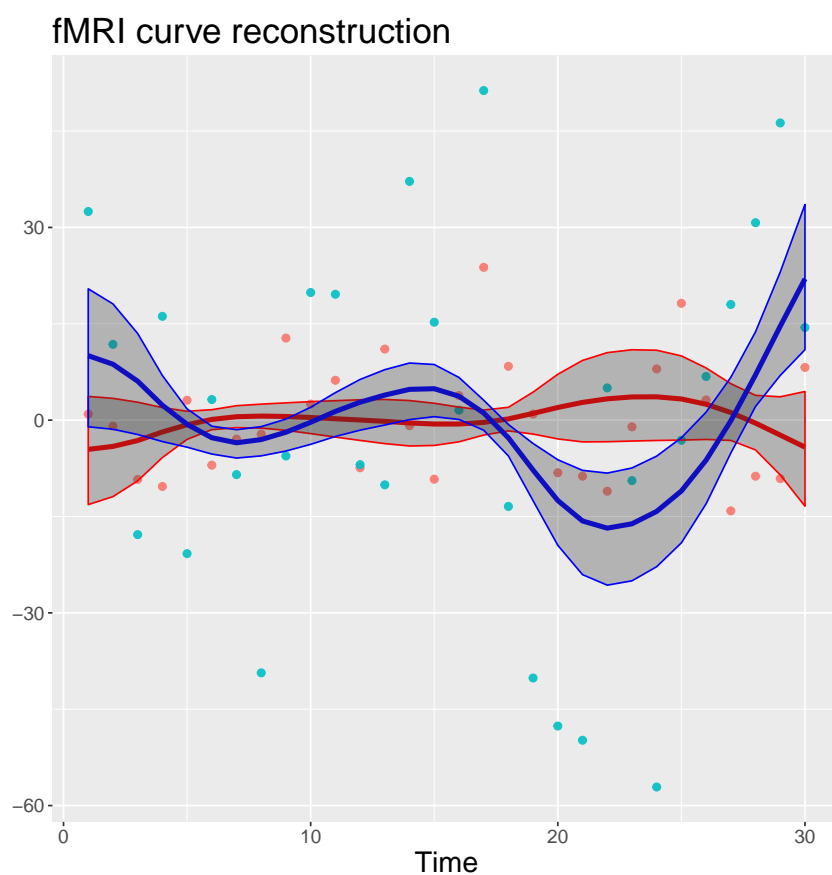


**Figure 11.** fMRI data analysis: posterior means and 95% credible bands for the resting-state fMRI data recorded from 2 sites in Frontal (red) and Occipital (blue) brain regions.

**Table 1**

*Simulation study: clustering performance of PCL-fPCA in DGP1. The table reports median and IQR of ARI (Adjusted Rand Index) computed for each MC dataset and every STN and eigendimension analysed.*

Eigendimension	<i>ARI</i>
<b>STN=1</b>	
<i>1st dim</i>	1 [1,1]
<i>2nd dim</i>	0.753 [0.444,0.868]
<b>STN=6</b>	
<i>1st dim</i>	1 [1,1]
<i>2nd dim</i>	0.966 [0.933,0.966]



**Table 2**

*fMRI data analysis - 4 different settings tested in the sensitivity analysis of the clusters precision  $s$  (or standard deviation  $\sigma$ ) and Dirichlet precision  $\alpha$  for each of the  $k = 3$  dimensions retained.*

dimension $k$	cluster variability	precision parameter
<b>1</b>		
$k1$	$s_1 \sim \Gamma(1, 1.5 \times \hat{\lambda}_1)$	$\alpha \sim U[0, 15]$
$k2$	$\sigma_2 \sim U[0, \sqrt{1.5 \times \hat{\lambda}_2}]$	$\alpha \sim U[0, 10]$
$k3$	$\sigma_3 \sim U[0, \sqrt{1.5 \times \hat{\lambda}_3}]$	$\alpha \sim U[0, 10]$
<b>2</b>		
$k1$	$s_1 \sim \Gamma(1, 0.5 \times \hat{\lambda}_1)$	$\alpha \sim U[0, 5]$
$k2$	$\sigma_2 \sim U[0, \sqrt{0.5 \times \hat{\lambda}_2}]$	$\alpha \sim U[0, 5]$
$k3$	$\sigma_3 \sim U[0, \sqrt{0.5 \times \hat{\lambda}_3}]$	$\alpha \sim U[0, 5]$
<b>3</b>		
$k1$	$s_1 \sim \Gamma(1, \hat{\lambda}_1)$	$\alpha \sim U[0, 10]$
$k2$	$s_2 \sim \Gamma(1, \hat{\lambda}_2)$	$\alpha \sim U[0, 10]$
$k3$	$s_3 \sim \Gamma(1, \hat{\lambda}_3)$	$\alpha \sim U[0, 10]$
<b>4</b>		
$k1$	$\sigma_1 \sim U[0, \sqrt{\hat{\lambda}_1}]$	$\alpha \sim U[0, 5]$
$k2$	$\sigma_2 \sim U[0, \sqrt{\hat{\lambda}_2}]$	$\alpha \sim U[0, 5]$
$k3$	$\sigma_3 \sim U[0, \sqrt{\hat{\lambda}_3}]$	$\alpha \sim U[0, 5]$

**Table 3**

*Simulation study: clustering performance. The table reports median and IQR of CII (Clustering Improvement Index) computed for each MC dataset and every STN and eigendimension analysed.*

Eigendimension	<i>CII</i>
<b>STN=1</b>	
<i>1st dim</i>	0.993 [0.993, 0.986]
<i>2nd dim</i>	0.645 [0.693, 0.523]
<b>STN=6</b>	
<i>1st dim</i>	0.962 [0.968, 0.950]
<i>2nd dim</i>	0.828 [0.855, 0.797]